Cell PRESS
Immunity
Article

Intestinal Lamina Propria Dendritic Cell Subsets Have Different Origin and Functions

Chen Varol,[1,5] Alexandra Vallon-Eberhard,[1,5] Eran Elinav,[1,2] Tegest Aychek,[1] Yami Shapira,[2] Hervé Luche,[3] Hans Jörg Fehling,[3] Wolf-Dietrich Hardt,[4] Guy Shakhar,[1] and Steffen Jung[1,*]
[1]Department of Immunology, The Weizmann Institute of Science, Rehovot, Israel 76100
[2]Gastroenterology and Hepatology Institute, Tel Aviv-Sourasky Medical Center, Tel Aviv, Israel
[3]Institute of Immunology, University Clinics Ulm, Ulm, Germany
[4]Institute of Microbiology, D-BIOL, ETH Zuerich, CH-8093 Zuerich, Switzerland
[5]These authors contributed equally to this work
*Correspondence: s.jung@weizmann.ac.il
DOI 10.1016/j.immuni.2009.06.025

SUMMARY

The intestinal immune system discriminates between tolerance toward the commensal microflora and robust responses to pathogens. Maintenance of this critical balance is attributed to mucosal dendritic cells (DCs) residing in organized lymphoid tissue and dispersed in the subepithelial lamina propria. In situ parameters of lamina propria DCs (lpDCs) remain poorly understood. Here, we combined conditional cell ablation and precursor-mediated in vivo reconstitution to establish that lpDC subsets have distinct origins and functions. CD103$^+$ CX$_3$CR1$^-$ lpDCs arose from macrophage-DC precursors (MDPs) via DC-committed intermediates (pre-cDCs) through a Flt3L growth-factor-mediated pathway. CD11b$^+$ CD14$^+$ CX$_3$CR1$^+$ lpDCs were derived from grafted Ly6C^{hi} but not Ly6C^{lo} monocytes under the control of GM-CSF. Mice reconstituted exclusively with CX$_3$CR1$^+$ lpDCs when challenged in an innate colitis model developed severe intestinal inflammation that was driven by graft-derived TNF-α-secreting CX$_3$CR1$^+$ lpDCs. Our results highlight the critical importance of the lpDC subset balance for robust gut homeostasis.

INTRODUCTION

Mononuclear phagocytes, including macrophages (Mϕs) and dendritic cells (DCs) are critically involved in the maintenance of tissue integrity, as well as in the initiation and control of innate and adaptive immunity. These dual activities are especially important in the mammalian intestinal mucosa, which is separated by a single columnar epithelial cell layer from the gut lumen (Artis, 2008). Specifically, the intestinal immune system has to maintain tolerance to harmless food antigens and commensal microorganisms, yet robustly respond to harmful pathogens. Dysregulation of this balance results in uncontrolled inflammatory disorders, such as inflammatory bowel disease (IBD) in humans (Xavier and Podolsky, 2007).

Intestinal mononuclear phagocytes are distributed in organized lymphoid organs, such as the Peyer's Patches (PPs) and mesenteric lymph nodes (MLNs), but also highly abundant in the loose connective tissue underlying the epithelium, the lamina propria (Niess et al., 2005; Coombes and Powrie, 2008; Iwasaki, 2007). Lamina propria DCs (lpDCs) first aroused attention when they were shown to penetrate epithelial tight junctions to sense and sample the gut lumen (Rescigno et al., 2001; Niess et al., 2005). Retinoic acid-producing CD103$^+$ lpDCs were reported to imprint α4β7 and CCR9 expression on naive lymphocytes to establish gut tropism, as well as to induce FoxP3$^+$ T regulatory cells (Coombes and Powrie, 2008). CD11b$^+$ lpDCs were found to promote TGFβ-dependent T helper 1 (Th1) and Th17 cell differentiation (Denning et al., 2007; Uematsu et al., 2008). The latter is also supported by a CD70$^+$ CD11b$^+$ lpDC subset driven by microflora-derived ATP (Atarashi et al., 2008). Furthermore, TLR5$^+$ CD11b$^+$ lpDCs were shown to induce IgA class switch recombination of B cells through provision of APRIL (Uematsu et al., 2008). Notably, these functional assays were performed ex vivo. It hence remains unclear whether these activities exist in the physiological tissue and microflora context and whether lpDCs act upon migration to the local draining MLN (Worbs et al., 2006) or display these activities within the lamina propria itself (Uematsu et al., 2008).

The phenotypic classification of lpDC subsets based on only CD103 and CD11b expression remains unsatisfactory. Given the recent progress in our understanding of the origins of splenic DCs (Geissmann et al., 2003; Fogg et al., 2006; Naik et al., 2006; Onai et al., 2007; Varol et al., 2007; Liu et al., 2007; Waskow et al., 2008; Liu et al., 2009), we hence sought to investigate the functional organization of lpDCs by probing their in vivo origins with a combination of conditional cell ablation and engraftment with defined DC precursors.

Here, we report the differential origin of the two main lamina propria DC subsets. CD103$^+$ CX$_3$CR1$^-$ lpDCs arose via nonmonocytic DC-committed intermediates (pre-cDCs) from MDPs through a Flt3L-driven pathway. In contrast, CD11b$^+$ CD14$^+$ CX$_3$CR1$^+$ lpDCs were exclusively derived from Ly6C^{hi} but not Ly6C^{lo} monocytes in a GM-CSF-controlled manner. Interestingly, during the reconstitution process CX$_3$CR1$^+$ lpDCs underwent massive clonal expansion in the lamina propria layer. Finally, we provide evidence that mice lacking CD103$^+$ CX$_3$CR1$^-$ lpDCs are uniquely sensitive to DSS-induced colitis because of the propensity of CX$_3$CR1$^+$ lpDCs to secrete TNF-α. Our data thus highlight the importance of a critical balance between

CD103$^+$ CX$_3$CR1$^-$ and CX$_3$CR1$^+$ lpDCs for tissue repair and gut homeostasis.

RESULTS

Phenotypic Characterization of Intestinal Lamina Propria Dendritic Cell Subsets

Lamina propria dendritic cells (lpDCs) of the mouse intestine have been divided into two main CD11b$^-$ CD103^{hi} and CD11b$^+$ CD103^{lo} subsets (Coombes et al., 2007; Denning et al., 2007; Jang et al., 2006; Sun et al., 2007; Uematsu et al., 2008). To further characterize the composition of the lpDC compartment of the small and large intestine, we took advantage of *Cx3cr1*$^{gfp/+}$ mice, in which one allele of the gene encoding the CX$_3$CR1 chemokine receptor has been replaced with a green fluorescent protein gene (*gfp*) (Jung et al., 2000). Notably, in both the colon and ileum of *Cx3cr1*$^{gfp/+}$ mice (Figure 1 and Figure S1A available online), CD11b$^-$ lpDCs were homogeneously CX$_3$CR1-GFP$^-$, whereas CD11b$^+$ lpDCs could be further divided into three distinct subsets according to size and CX$_3$CR1-GFP expression: FSC^{hi} CX$_3$CR1-GFP^{hi}, FSC^{int} CX$_3$CR1-GFP^{lo}, and FSC^{lo} CX$_3$CR1-GFP$^-$ cells (Figure 1). CD11b$^+$ and CX$_3$CR1-GFP$^+$ CD11b$^-$ lpDCs differed considerably with respect to surface-marker expression. CD11b$^-$ lpDCs were CD103^{hi} CD14$^-$ CD8^{lo}, whereas CX$_3$CR1-GFP$^+$ CD11b$^+$ lpDCs (G4 and G5) were CD103$^{-/lo}$ CD14$^+$ CD8$^-$. The latter subsets, whose CD11c expression was lower than that on CD11b$^-$ lpDCs, also expressed higher levels of the costimulatory molecules CD80, CD86, and CD70. Interestingly, CX$_3$CR1-GFP$^-$ CD11b$^+$ lpDCs were CD103^{hi} and CD14$^-$ and thus more similar to the CD11b$^-$ lpDC population than the CX$_3$CR1/GFP$^{lo\text{-}hi}$ CD11b$^+$ subsets (Figure 1 and Table S1). Flow cytometric analysis of isolated small intestinal villi confirmed the existence of both CD11b$^-$ and CD11b$^+$ lpDCs in the lamina propia (Figure S1B).

Differential Origin of CD11b$^+$ and CD11b$^-$ lpDCs

Using conditional DC ablation and a complementary adoptive precursor cell transfer strategy, we previously showed that grafted monocytes differentiate in the ileal lamina propria of DC-depleted recipient mice into CD11c^{hi} cells (Varol et al., 2007). The ablation system used in these studies involved CD11c-DTR transgenic mice that carry a human diphtheria toxin receptor (DTR) transgene under the murine CD11c promoter, thereby allowing the inducible ablation of CD11c^{hi} DCs (Jung et al., 2002). Bone marrow (BM) chimeras generated through reconstitution of irradiated WT recipient mice with CD11c-DTR BM tolerate repeated DTx injection without adverse side effects, allowing for prolonged DC ablation without major inflammation (Zaft et al., 2005). In our original study, monocyte-graft-derived cells were largely CX$_3$CR1-GFP^{hi}, but also included some CX$_3$CR1-GFP^{lo} cells (Varol et al., 2007). Given the above refined lpDC characterization, we performed comprehensive adoptive transfers of CD45.1 *Cx3cr1*$^{gfp/+}$ precursor cells into DC-depleted recipients (CD45.2). DTx treatment of [CD11c-DTR > WT] chimeras resulted in the depletion of all lpDC subsets, whereas the population of CD11c$^{-/\,lo}$ CD11b$^+$ lpMΦ remained unaltered (Figure 2A). Interestingly, FACS analysis of the recipient's colonic lamina propria at day 14 after transfer revealed that *Cx3cr1*$^{gfp/+}$ Ly6C^{hi} monocytes differentiated into CD45.1$^+$ CD11b$^+$ but not

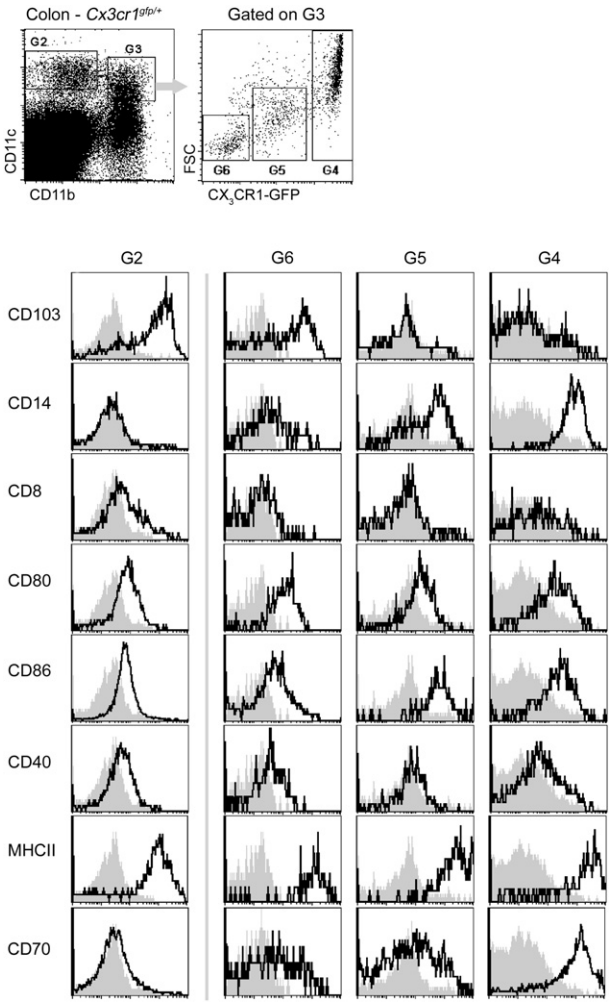

Figure 1. Phenotypic Characterization of Colonic lpDCs

Flow cytometry analysis of colonic lpDC compartment of *Cx3cr1*$^{gfp/+}$ mice. Top dot blots show division of CD11c^{hi} lpDCs into two major CD11b$^-$ (G2) and CD11b$^+$ (G3) subpopulations. CD11b$^+$ lpDCs were further subdivided into FSC^{hi} GFP^{hi} (G4), FSC^{int} GFP^{lo} (G5), and FSC^{lo} GFP$^-$ cells (G6). Histograms show expression of indicated surface markers by different subsets. Data are representative of three independent experiments.

into CD11b$^-$ lpDCs. Moreover, Ly6C^{hi} monocytes gave rise to CX$_3$CR1-GFP^{hi} and CX$_3$CR1-GFP^{lo} but not CX$_3$CR1-GFP$^-$ CD11b$^+$ lpDCs (Figure 2B). Ly6C^{hi} monocyte-derived CD11b$^+$ lpDCs featured surface marker comparable to that of the corresponding steady-state lpDC population, including CD14 and CD80 expression (Figure 2B). These results establish that Ly6C^{hi} monocytes are in our experimental system precursors of CX$_3$CR1-expressing CD11b$^+$ lpDCs, but not the CD11b$^-$ lpDCs. Notably, adoptively transferred Ly6C^{lo} monocytes failed to reconstitute ileal and colonic lpDCs of DC-depleted mice (Figures S2A and S2B and data not shown). Ly6C^{lo} monocytes gave, however, rise to Peyer's Patch DCs, although these cells were morphologically distinct from the ones generated from Ly6C^{hi} monocytes (Figures S2C and S2D).

To elucidate the in vivo origin of the CD11b$^-$ lpDCs, we adoptively transferred macrophage-DC precursors (MDPs) (Fogg

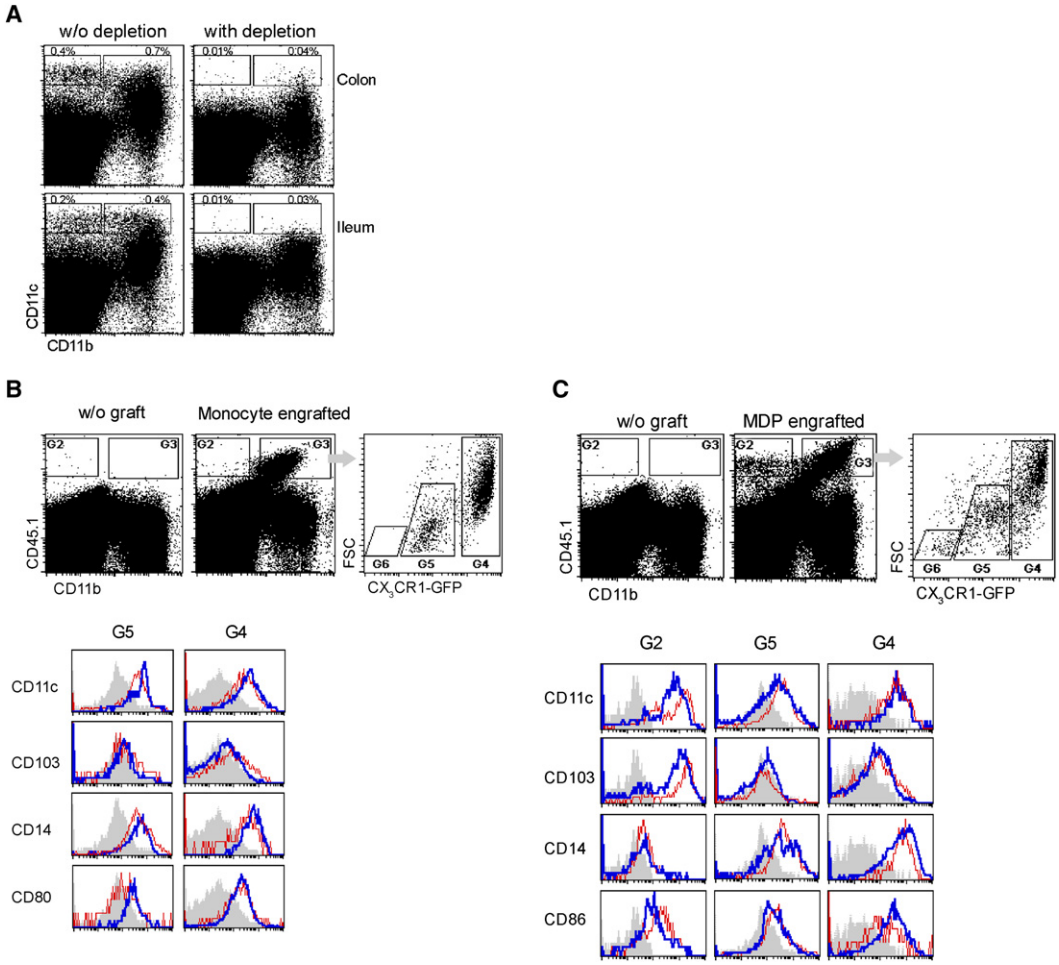

Figure 2. In Vivo Reconstitution Revealing Differential lpDC Origins

(A) Flow cytometry analysis documenting DTx-induced lpDC ablation from ileum of [CD11c-DTR > WT] BM chimeras. Data are representative of six independent experiments.

(B) Flow cytometry analysis of colonic lpDC compartment of DC-depleted mice (CD45.2) with or without engraftment of Ly6C^{hi} monocytes (*Cx3cr1*$^{gfp/+}$ CD45.1) (1.5 × 10^6 cells; purity: 95%). Mice were analyzed 2 weeks after transfer. Data are representative of three independent experiments.

(C) Flow cytometry analysis of colonic lpDC compartment of DC-depleted mice (CD45.2) with or without engraftment of MDPs (*Cx3cr1*$^{gfp/+}$ CD45.1) (2 × 10^5 cells; purity: 95%). Mice were analyzed 2 weeks after transfer. Lower histograms in (B) and (C) indicate surface-marker expression of indicated subsets of graft-derived (blue line) and steady-state DC subpopulations of control animals (red line). Filled gray histograms represent isotype control. Data are representative of three independent experiments.

et al., 2006) into DC-depleted mice (CD45.2). Flow cytometry analysis of the recipients' colonic lamina propria 2 weeks after transfer revealed that MDPs, isolated from *Cx3cr1*$^{gfp/+}$ CD45.1 mice, reconstituted both CD11b$^-$ and CD11b$^+$ lpDCs, including the CX$_3$CR1-GFP$^-$ CD11b$^+$ lpDC subpopulation (Figure 2C). Flow cytometry analysis of the MDP-derived CD11b$^-$ lpDCs confirmed their phenotypic resemblance to steady-state CD11b$^-$ lpDCs (Figure 2C). Analysis of the ileal lamina propria of monocyte recipients yielded similar results, whereas the ileum of MDP recipients showed more CX$_3$CR1-GFP^{int} CD11b$^+$ than CX$_3$CR1-GFP^{hi} CD11b$^+$ lpDCs (Figures S2A and S2B). Fluorescent microscopical imaging revealed graft-derived CX$_3$CR1-GFP^{hi} cells at day 14 after the engraftment of lpDC-depleted mice with Ly6C^{hi} monocytes or MDPs, but not Ly6C^{lo} monocytes, in the lamina propria of both colon and ileum of the recipient mice (Figures S3A and S3B). These data suggested that CD11b$^-$ lpDCs arise from MDPs via nonmonocytic circulating precursor cells. To define this immediate progenitor of CD11b$^-$ lpDCs, we performed adoptive transfers with recently reported DC-committed precursors (pre-cDCs) (Liu et al., 2009). As shown in Figure 3, grafted pre-cDCs predominantly gave rise to CD11c^{hi} CX$_3$CR1$^-$ but not CD11c^{int} CX$_3$CR1^{hi} lpDCs. Grafted MDPs gave rise to both CX$_3$CR1$^-$ and CX$_3$CR1$^+$ lpDC populations and grafted Ly6C^{hi} monocytes gave rise only to CX$_3$CR1$^+$ lpDCs. Collectively, these data establish that CD103$^+$ and CX$_3$CR1$^+$ lpDCs are derived from distinct precursors.

CD11b$^-$ and CD11b$^+$ lpDC Generation Depend on Flt3L and GM-CSF, Respectively

The finding that CD11b$^-$ and CD11b$^+$ lpDCs rely on distinct precursor cells for their reconstitution implies their distinct ontogeny. Recent data highlight the critical role of GM-CSF

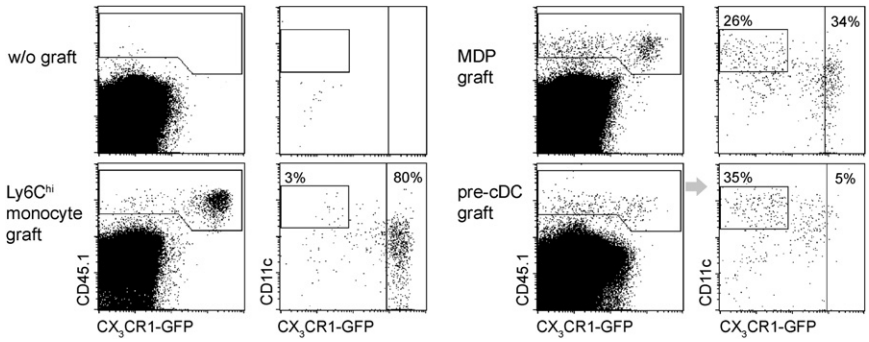

Figure 3. Definition of Immediate lpDC Precursors

Flow cytometry analysis of colonic lpDC compartment of DC-depleted mice (CD45.2) with or without engraftment of monocytes (10^6), MDPs (10^5), and pre-cDCs (10^5) (*Cx3cr1*$^{gfp/+}$ CD45.1). Data are representative of two independent experiments.

and Flt3L in DC differentiation pathways (Daro et al., 2000; Miller et al., 2002; Karsunky et al., 2003; Miller et al., 2003; Hieronymus et al., 2005; Waskow et al., 2008). To elucidate the involvement of these factors in the generation of CD11b$^-$ and CD11b$^+$ lpDCs, we analyzed the potential of GM-CSF receptor-deficient (*Csf2a*$^{-/-}$) and *Flt3*$^{-/-}$ precursor cells to give rise to the two lpDC subsets. Analysis of the lamina propria of the respective mutant mice revealed a reciprocal effect on the distribution of the lpDC subsets (Figure S4A). To compare the contribution of the respective cytokine-receptor-deficient lpDCs to WT lpDCs within the same animal, we generated mixed BM chimeras with WT and *Csf2a*$^{-/-}$ or *Flt3*$^{-/-}$ BM that could be distinguished according to an allotypic CD45 marker (Mackarehtschian et al., 1995; Robb et al., 1995). FACS analysis revealed decreased numbers of CD11b$^+$ and CD11b$^-$ lpDCs in the *Csf2a*$^{-/-}$ and *Flt3*$^{-/-}$ lpDC populations, respectively. The corresponding WT lpDC populations were unskewed, indicating that the effects were cell intrinsic (Figure 4A).

To validate these findings, we tested the effect of excess GM-CSF or Flt3L on the lpDC distribution. To this end, we inoculated WT mice with B16 tumor cells genetically manipulated to express GM-CSF (B16-GM-CSF) or Flt3L (B16-Flt3L) (Mach et al., 2000). Flow cytometry analysis revealed a profound increase of the CD11b$^+$ lpDC subset specifically in B16-GM-CSF bearing mice, whereas B16-Flt3L-bearing mice displayed an expansion of the CD11b$^-$ lpDC subset (Figure 4B), as compared with mice harboring the parental B16 tumor.

To further investigate the effects of GM-CSF or Flt3L on lpDC precursors, we performed a transient depletion of lpDCs in CD11c-DTR mice and allowed for self-reconstitution of the lpDC compartment from endogenous precursors. For 10 days, the mice received daily intraperitoneal (i.p.) injections of supernatants isolated from B16, B16-GM-CSF, or B16-Flt3L cultures. Exposure of the mice during the reconstitution phase to exogenous GM-CSF and Flt3L skewed the lpDC balance toward the CD11b$^+$ and CD11b$^-$ colonic lpDCs, respectively (Figure S4B). Cumulatively, these results suggest that the generation of monocyte-derived CD11b$^+$ lpDCs is controlled by GM-CSF, whereas pre-cDC-derived CD11b$^-$ lpDCs originate through a Flt3L-driven pathway (Figure S5).

Ly6C^{hi} Monocyte-Derived CD11b$^+$ lpDCs Arise through Clonal Expansion

Fluorescent microscopy analysis of the monocyte recipients revealed the progressive replenishment of the lamina propria by CX$_3$CR1-GFP$^+$ cells until day 14, after which they gradually disappeared (Figures S6A and S6B). In the ileum, the number of graft-derived lpDCs gradually increased from an average of one to two cells/villus (day 2) up to nearly full reconstitution, suggesting that lpDCs might have undergone proliferation (Figure S6B). Supporting this notion, transferred CFSE-labeled CD45.1 monocytes differentiated into CD11c^{hi} CD11b$^+$ lpDCs already at day 2, but gradually lost CFSE only from day 4 on, indicating cell division (Figure S6C). With fluorescent video endoscopy, similar replenishment kinetics were detected in individual monocyte recipients over time (Movie S1).

Notably, transfers of *Cx3cr1*$^{gfp/+}$ monocytes and MDPs consistently resulted in a patchy reconstitution of the recipient's villi (Figure 5A). This could be due to uneven precursor recruitment to specific villi or to clonal expansion of single-monocyte-derived cells that seeded given villi. To investigate the latter option, we performed a transfer with a 1:1 mixture of monocytes that yield either green fluorescent lpDCs (*Cx3cr1*$^{gfp/+}$ monocytes) or red fluorescent lpDCs (CD11c-Cre:R26tdRFP monocytes) (Caton et al., 2007; Luche et al., 2007). This mixed graft resulted in the generation of villi that were, by large, exclusively repopulated by green or red fluorescent lpDCs (Figure 5B). Moreover, even when villi were seeded by both tdRFP$^+$ and GFP$^+$ lpDCs, the two distinctly labeled populations were organized into clusters, suggesting clonal expansion. Discrete GFP- and tdRFP-positive patches in the lpDC network were also observed in other regions, such as the colon, duodenum, jejunum, and cecum (Figure 5C and data not shown). Transfers of mixed monocyte grafts into DTx-treated nonchimeric CD11c-DTR recipients yielded similar results (Figures S7A and S7B). Collectively, these findings establish that in our experimental system, individual villi are seeded with a limited number of circulating monocytes and that the resulting monocyte-derived lpDCs arise through proliferative DC expansion.

Grafted-Monocyte-Derived lpDCs Restore DC Functions

Small intestinal lpDCs can penetrate the intestinal epithelium and send trans-epithelial dendrites (TEDs) toward the gut lumen to sense or sample luminal pathogens (Rescigno et al., 2001; Chieppa et al., 2006), and TEDs can be readily visualized in the lamina propria of *Cx3cr1*$^{gfp/+}$ mice (Niess et al., 2005; Vallon-Eberhard et al., 2006). Microscopic analysis of the terminal ileum of DC-depleted monocyte recipients revealed that graft-derived CD11b$^+$ lpDCs formed frequent TEDs (Figure 6A).

We recently showed that virulence of the *Salmonella typhimurium* SL1344 *invG* mutant strain lacking a functional type 3 secretion system critically requires lpDCs for transepithelial invasion

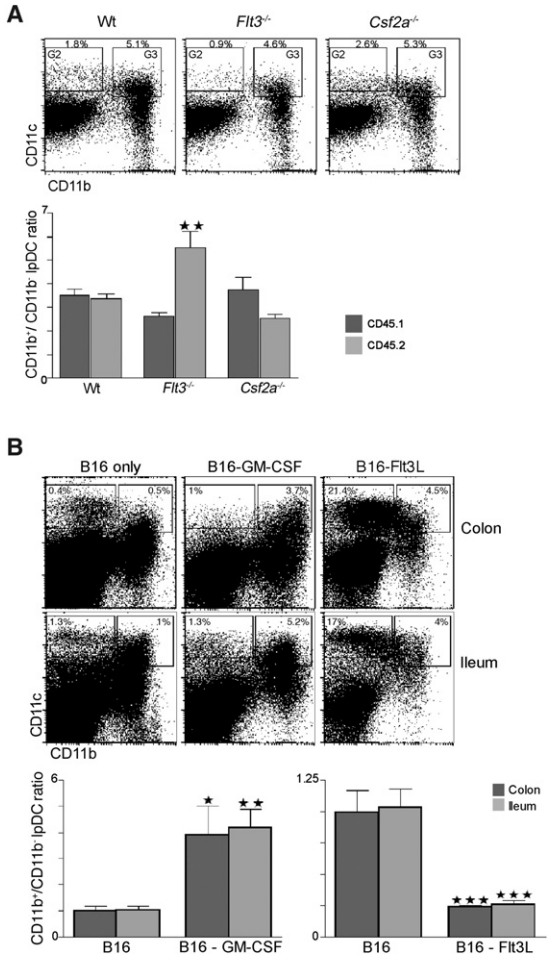

Figure 4. CD11b$^-$ and CD11b$^+$ lpDC Generation Depend on Flt3L and GM-CSF, Respectively

(A) Flow cytometry analysis of lpDC frequencies and a bar graph summarizing ratios of CD11b$^+$ and CD11b$^-$ DCs in the colonic lamina propria of mixed BM chimeras reconstituted with 50% WT BM (CD45.1) and BM isolated from WT, *Csf2a*$^{-/-}$, or *Flt3*$^{-/-}$ mice (CD45.2). Dark-gray columns represent WT CD45.1 lpDC fractions; light-gray columns represent CD45.2 lpDC fractions. (n = 4–5 for each group; Student's t test, in comparison to corresponding CD45.1 WT fraction, CD45.2 *Flt3*$^{-/-}$: **p = 0.003; CD45.2 *Csf2a*$^{-/-}$: p = 0.052). CD45.2 WT mean: 3.38 ± 0.21; CD45.2 *Flt3*$^{-/-}$ mean: 5.54 ± 0.68; and CD45.2 *Csf2a*$^{-/-}$ mean: 2.64 ± 0.18.

(B) Flow cytometry analysis of lpDC frequencies and a bar graph summarizing ratios of CD11b$^+$ to CD11b$^-$ DCs in the colonic (dark gray) and ileal (light gray) lamina propria of *Cx3cr1*$^{gfp/+}$ mice 14 days after s.c. injection of B16, B16-GM-CSF, or B16-Flt3L tumor cells (n = 4 for each group; Student's t test, in comparison with parental B16; B16-GM-CSF: colon *p = 0.016, ileum **p = 0.009; B16-Flt3L: colon ***p = 0.0004, ileum ***p < 0.0001). B16 mean: 0.99 ± 0.17; B16-Flt3L mean: 0.24 ± 0.01; and B16-GM-CSF mean: 3.91 ± 1.1.

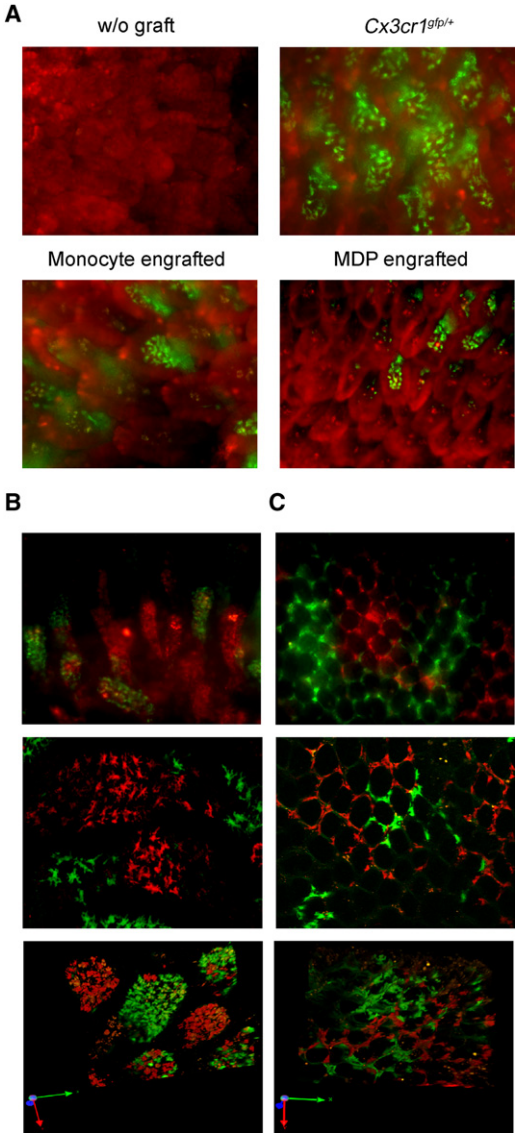

Figure 5. Clonal Expansion of Ly6C^{hi} Monocyte- and MDP-Derived CX$_3$CR1^{hi} CD11b$^+$ lpDCs

(A) Fluorescent microscopy image analysis of CMTMR-labeled ileal lamina propria on day 7 after adoptive transfer of Ly6C^{hi} *Cx3cr1*$^{gfp/+}$ monocytes (1.5 × 10^6 cells; purity: 95%) and MDPs (2 × 10^5 cells; purity: 95%). Reconstituted villi are populated with GFP$^+$ lpDCs.

(B and C) Fluorescent microscopic (left panel), confocal microscopic (middle panel), and 2P (right panel) imaging analysis of ileal and colonic lamina propria of DC-depleted recipients 7 days after engraftment with mixture of monocytes yielding GFP$^+$ and tdRFP$^+$ lpDCs. (C) shows original magnifications 10× and 20×. Data are representative of three independent experiments.

(Hapfelmeier et al., 2008). Indeed, lpDC-depleted mice featured a markedly reduced intestinal *Salmonella* uptake. Notably however, the colonic invasion of mutant *Salmonella* was reconstituted in mice that had received a monocyte graft (Figure 6B).

Our analysis revealed that grafted monocytes also gave rise to CD11b$^+$ DCs in MLNs (Figure S8). We therefore next investigated the functional role of graft-derived DCs in T cell priming. To this end, we transferred ovalbumin (OVA)-specific TCR transgenic CD4$^+$ T cells (OT-II) (Barnden et al., 1998) into untreated and lpDC-depleted recipient mice. The T cell graft carried an allotypic marker (CD45.1) and was labeled with CFSE, thus allowing detection and assessment of in vivo proliferation, respectively. FACS analysis of MLNs revealed that the grafted T cells readily proliferated upon oral OVA challenge in the WT mice, whereas T cell expansion was abrogated in DC-depleted mice. DC restoration by prior monocyte transfer reconstituted the CD4$^+$ T cell

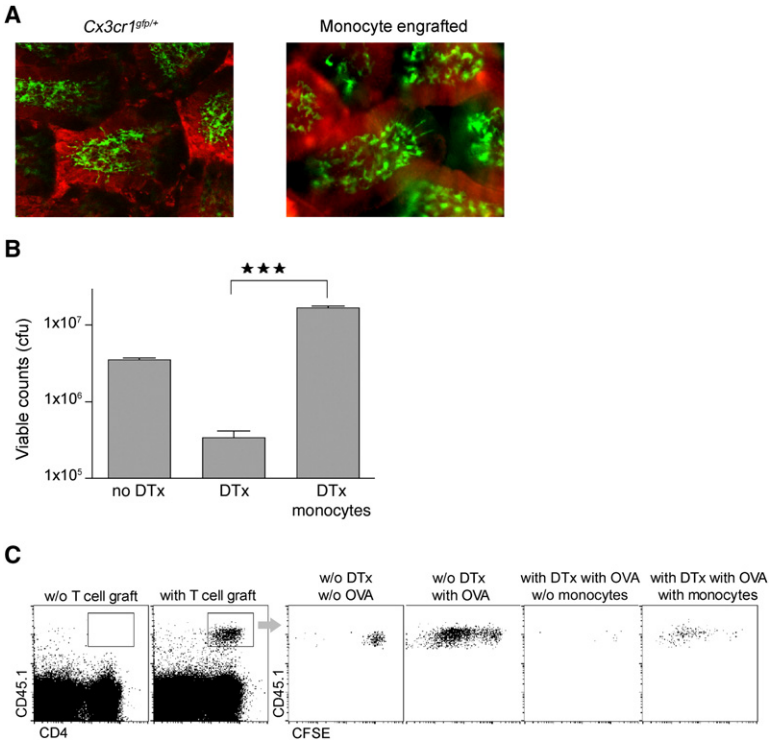

Figure 6. Monocyte-Graft-Derived lpDCs Restore Host lpDC Functions

(A) Confocal imaging analysis of TED formation by monocyte-derived lpDCs after oral TLR7 agonist challenge (Imiquimod: 20 μg) in DC-depleted recipients (graft 1.5 × 10^6 cells; purity: 95%) 2 weeks after transfer. Original magnification 20×. Data are representative of three independent experiments.

(B) Bar graphs representing colon load of mutant *Salmonella typhimurium* (strain SB161) (challenge 5 × 10^6 CFU; n = 5 for each group; Student's t test, **p = 0.003). Data are representative of two independent experiments. No DTx mean: 3483000 ± 241400; DTx only mean: 338000 ± 79210; and DTx with monocytes mean: 17017000 ± 651880.

(C) Flow cytometry analysis of MLNs of WT and DC-depleted mice that underwent adoptive transfer of CFSE-labeled OT-II $CD4^+$ T cells (CD45.1) with or without engraftment with $Ly6C^{hi}$ monocytes. Data are representative of two independent experiments.

priming (Figure 6C). Taken together, these results establish that $Ly6C^{hi}$ monocytes differentiate in the intestinal lamina propria and in the associated lymphoid tissue into functional DCs.

Impaired Balance of $CD11b^+$ and $CD11b^-$ lpDCs Predisposes to Colitis Development

LpDCs are considered critical players in the maintenance of gut homeostasis. In addition, defective lpDC functions and hyperresponsiveness to microflora are considered a major cause for IBD (Coombes and Powrie, 2008). Reconstitution of DC-depleted mice with monocyte grafts resulted in a pronounced imbalance of the $CD11b^+$ versus the $CD11b^-$ lpDC subsets (Figure 2B), but histological analysis revealed no signs of inflammation (Figure S9). To probe the robustness of gut homeostasis, we challenged monocyte recipients by oral administration of dextran sulfate sodium (DSS). This established colitis model is characterized by ulceration and submucosal inflammation provoked by disruption of the epithelial barrier and exposure to luminal microbiota (Okayasu et al., 1990). Notably, if DSS is given transiently and at low doses, WT mice tolerate the acute DSS-inflicted damage and restore epithelial integrity (Cooper et al., 1993). To study the role of the $CD11b^+$/$CD11b^-$ lpDC balance on the initiation phase of colitis, we added DSS (1%) to the drinking water of DC-depleted and monocyte-reconstituted mice on day 9 after transfer for 1 week and then analyzed them by colonoscopy and histology for colitis severity.

Upon DSS challenge, all mice that were not DC depleted, persistently DC depleted, or transiently DC depleted and left to self-reconstitute both $CD11b^+$ and $CD11b^-$ lpDCs developed only mild intestinal inflammation. In contrast, mice reconstituted with monocytes exhibited hallmarks of severe colitis, as evaluated and quantified by colonoscopy (Becker et al., 2006; Becker et al., 2005) (Figures 7A and 7B and Movie S2). Histology examination showed widespread colitis lesions exclusively in mice reconstituted with monocytes (Figure 7C). These results suggest that monocyte-derived $CD11b^+$ lpDCs display proinflammatory properties that impede tissue repair and highlight the importance of the lpDC balance for robust gut homeostasis. This notion is further supported by the fact that also mice whose lpDC compartment was skewed toward $CD11b^+$ lpDCs as a result of the Flt3 deficiency were found more susceptible to DSS-induced colitis (Figure S10).

Anti-TNF-α treatment ameliorates disease progression in humans with IBD and murine colitis models (Abe et al., 2007; Berndt et al., 2007; Garrett et al., 2007), and this cytokine might also be responsible for the proinflammatory activity in our system. To specifically test the involvement of monocyte-derived TNF-α-producing $CD11b^+$ lpDCs, we reconstituted lpDC-depleted mice with TNF-α-deficient monocytes (Pasparakis et al., 1996). In contrast to WT monocyte recipients, mice engrafted with $Tnf^{-/-}$ monocytes develop only mild colitis upon DSS treatment (Figures 7B–7D). To confirm the lpDC reconstitution by the $Tnf^{-/-}$ lpDCs, we took advantage of the fact that intestinal IL-12 p40 expression is restricted to lpDCs in steady state (Becker et al., 2003). Accordingly, IL-12 p40 transcripts were undetectable by RT-PCR analysis in DC-depleted colons (Figure 7E). Notably, however, IL-12 p40 transcripts were readily detected in colonic tissue of mice that were allowed to self-reconstitute or that reconstituted with WT or $Tnf^{-/-}$ monocyte-derived lpDCs (Figure 7D). Cumulatively, these findings highlight the importance of a balanced lpDC compartment and establish that $Ly6C^{hi}$ monocyte-derived $CD11b^+$ lpDCs exacerbate colitis by secreting the proinflammatory cytokine TNF-α.

DISCUSSION

In our experiments, we used a combination of conditional cell ablation and precursor cell engraftment to investigate the origin and function of murine intestinal lamina propria DCs (lpDCs) in physiological context. We demonstrate that $CD103^+$

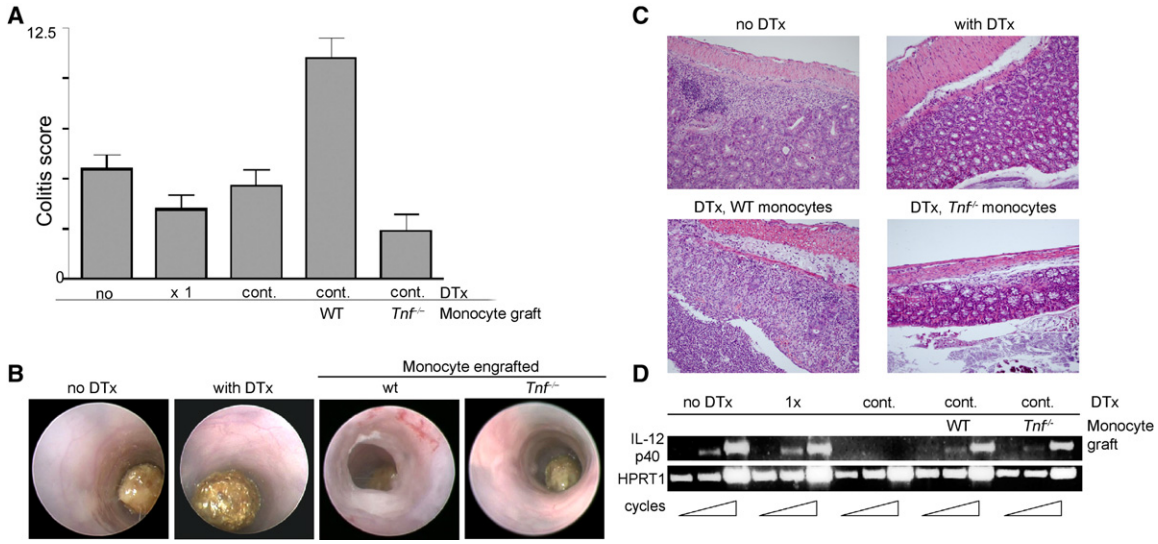

Figure 7. TNF-α-Producing Monocyte-Derived CD11b$^+$ lpDCs Induce Colitis after DSS Treatment

(A) Bar graphs representing colitis index as evaluated by colonoscopy of mice that were not DC depleted; persistently DC depleted; transiently DC depleted (and left to self-reconstitute); or persistently DC depleted and engrafted with WT or *Tnf*$^{-/-}$ monocytes (n = 5 for each group) that received DSS. Data are representative of three independent experiments. No DTx mean: 5.4 ± 0.75; DTx x 1 mean: 3.4 ± 0.75; cont. DTx mean: 4.6 ± 0.81; and cont. DTx with WT monocytes mean: 11 ± 0.97; cont. DTx with *Tnf*$^{-/-}$ monocytes mean: 2.33 ± 0.88.

(B) Representative colonoscopy images of indicated DSS-treated mice that were not DC depleted, persistently DC depleted, and persistently DC depleted and engrafted with WT or *Tnf*$^{-/-}$ monocytes.

(C) Corresponding H&E histology of DSS- induced colitis. Data are representative of three independent experiments.

(D) RT-PCR analysis for IL-12 p40 message performed on cDNA of tissue mRNA isolated from mice that were not DC depleted, transiently DC depleted (and left to self-reconstitute), persistently DC depleted, and persistently DC depleted and engrafted with WT or *Tnf*$^{-/-}$ monocytes (after the colonoscopy). Data are representative of two independent experiments.

CX_3CR1^- lpDCs originate through a DC-committed nonmonocytic intermediate from macrophage-DC precursors (MDPs); this differentiation pathway is uniquely driven by Flt3L. In contrast, CD11b$^+$ CD14$^+$ CX_3CR1^+ lpDCs derived from Ly6C^{hi} but not Ly6C^{lo} monocytes promoted by GM-CSF, and their derivation involved extensive local DC expansion in the mucosa. Functionally, our results highlight the critical importance of the lpDC subset balance for robust intestinal homeostasis. Thus, when challenged in an acute DSS-induced colitis model, mice that harbored exclusively monocyte-derived CX_3CR1^+ lpDCs failed to cope with the epithelial damage and developed severe intestinal inflammation, a process that was dependent on lpDC secretion of TNF-α.

Recent studies established that the murine intestinal lamina propria contains two major DC subsets: CD11b$^-$ CD103^{hi} and CD11b$^+$ CD103$^{-/lo}$ cells (Denning et al., 2007; Jang et al., 2006; Sun et al., 2007; Uematsu et al., 2008). Our present examination of the ileal and colonic lamina propria of *Cx3cr1*$^{gfp/+}$ mice revealed further lpDC complexity. Whereas CD11b$^-$ CD103^{hi} lpDCs were homogenously CX_3CR1-GFP$^-$, CD11b$^+$ lpDCs could be subdivided into three distinct subsets, on the basis of CX_3CR1 expression. CX_3CR1^- lpDCs, including CD11b$^-$ and CD11b$^+$ cells, were found to be CD103^{hi}, CD14$^-$, and CD8^{lo}. CX_3CR1^+ lpDCs were mostly negative for CD103 and CD8 and expressed high levels of CD14 and the costimulatory molecules CD80, CD86, and CD70.

To define lpDC origins, we resorted to an established depletion and reconstitution strategy (Varol et al., 2007). Adoptive transfers of MDPs yielded both CD103$^+$ CX_3CR1^- and CD14$^+$ CX_3CR1^+ lpDCs, although the lpDC compartment was consistently skewed toward CX_3CR1^+ lpDCs and thus did not restore homeostasis. Transfers of the immediate blood circulating precursors established that CD103$^+$ CX_3CR1^- lpDCs arouse from recently reported DC-committed precursors (pre-cDCs) (Liu et al., 2009), whereas CD14$^+$ CX_3CR1^+ lpDCs were derived from Ly6C^{hi} but not Ly6C^{lo} monocytes. Notably, our experimental system involves the ablation of endogenous lpDCs and it remains unclear whether and how this manipulation affects the generation of CX_3CR1^+ lpDCs from monocytes. However, monocytes were previously demonstrated to give rise to mucosal CD11b$^+$ DCs in the lung (Jakubzick et al., 2008; Landsman et al., 2007; Varol et al., 2007) and in the vagina (Iijima et al., 2007).

Recent studies have highlighted the critical role of the growth factors GM-CSF and Flt3L for the in vitro and in vivo generation of murine DCs (Daro et al., 2000; Hieronymus et al., 2005; Karsunky et al., 2003; Miller et al., 2003; Miller et al., 2002; Waskow et al., 2008). Our findings lend further support to a dichotomy of the DC compartment, where GM-CSF and MCSF drive the differentiation of monocytic precursor cells and their descendants, whereas Flt3L drives an alternative, monocyte-independent differentiation pathway that involves DC-committed precursors (pre-cDCs). We thus demonstrate opposing effects of GM-CSF and Flt3L on the differentiation of the lpDC subsets. *Csf2a*$^{-/-}$ mice displayed a significant decrease in CD11b$^+$ lpDCs, whereas there were fewer CD11b$^-$ lpDCs in [*Flt3*$^{-/-}$ > WT] chimeric mice. Analysis of BM chimeras harboring WT and mutant lpDCs

confirmed that both cytokines uniquely control the differentiation of CD103$^+$ and CX$_3$CR1$^+$ lpDCs in a cell-intrinsic manner. Addition of exogenous Flt3L and GM-CSF skewed the differentiation toward CD103$^+$ and CX$_3$CR1$^+$ lpDC subsets, respectively. Notably, the growth factors could have effects on lpDC precursor generation in the BM or act locally.

The intestinal reconstitution kinetics of CX$_3$CR1$^+$ lpDCs revealed a progressive replenishment that peaked after 2 weeks and resulted from proliferative lpDC expansion. Individual ileal recipient villi were reconstituted by discrete cell clones. The physiological relevance of this finding remains to be shown, yet it may potentially relate to the pathogenesis of the patchy discontinuous inflammation noted in IBD, mainly Crohn's disease (Vasquez et al., 2007). In agreement with our findings, it was reported that CD103$^-$ CD11b$^+$ lpDCs are maintained in part through homeostatic proliferation (Jaensson et al., 2008). Whereas our experimental approach precluded addressing the proliferative potential of CD103$^+$ lpDCs, this study indicated that the maintenance of CD103$^+$ ileal lpDCs relied on circulating BM-derived precursors, rather than on local proliferation (Jaensson et al., 2008). Our results suggest that these cells are the pre-cDCs.

The combination of lpDC ablation and precursor-mediated reconstitution allows the study of the impact of graft-derived lpDCs on the maintenance of gut homeostasis in a steady state and under challenge. Interestingly, mice persistently or transiently depleted of lpDCs neither developed spontaneous intestinal inflammation nor were overtly susceptible to colitis development. In contrast, mice that predominantly harbored monocyte-derived CX$_3$CR1$^+$ CD11b$^+$ DCs in their lamina propria developed severe signs of colitis in response to DSS challenge, as determined by colonoscopy and histological examination. This suggests that CX$_3$CR1$^+$ lpDCs interfere with the restoration of epithelial integrity that limits progression to chronic gut inflammation. Through adoptive transfer of mutant monocytes, we showed that this proinflammatory activity was critically dependent on TNF-α, thus corroborating earlier reports of the central role of this cytokine in innate and T cell-mediated colitis, as well as in human IBD (Abe et al., 2007; Berndt et al., 2007; Garrett et al., 2007). Our results establish that the inflammation resulting from the DSS-inflicted epithelial damage is caused by immune cells, and represents an innate immunopathology driven by CX$_3$CR1$^+$ lpDCs. They highlight the importance of a delicate balance between lpDCs subsets to maintain robust intestinal homeostasis that defies disturbances, as those induced by the breach of the epithelial barrier. These findings further suggest that CD103$^+$ CX$_3$CR1$^-$ lpDCs might harbor regulatory functions, which are required to curb the activities of CX$_3$CR1$^+$ CD11b$^+$ lpDCs. In support of this notion, CD103$^+$ lpDCs were reported to produce anti-inflammatory cytokines, such as TGF-β and IL-10 (Denning et al., 2007). It remains, however, to be shown whether CD103$^+$ lpDCs act directly on CX$_3$CR1$^+$ lpDCs or indirectly by affecting other immune cells or the epithelium itself.

In conclusion, we establish the differential origin of the two main lamina propria DC subsets. CD103$^+$ CX$_3$CR1$^-$ lpDCs arise, via a DC-committed nonmonocytic intermediate (pre-cDCs), from MDPs through an Flt3L-driven pathway. In contrast, CD14$^+$ CX$_3$CR1$^+$ lpDCs originated exclusively from Ly6C^{hi} but not Ly6C^{lo} monocytes in a GM-CSF-controlled manner. Mice lacking CD103$^+$ lpDCs were uniquely sensitive to DSS-induced colitis, highlighting the importance of a critical balance between lpDC subsets for tissue repair and robust gut homeostasis.

EXPERIMENTAL PROCEDURES

Animals

The study involved the use of the following 8- to 14-week-old mice: wild-type (WT) C57BL/6 mice, heterozygote mutant *Cx3cr1*$^{gfp/+}$ mice (Jung et al., 2000), CD11c-DTR transgenic mice (B6.FVB-Tg [Itgax-DTR/GFP] 57Lan/J) (Jung et al., 2002), Rosa26-tdRFP transgenic mice (Luche et al., 2007) crossed with CD11c-cre transgenic mice (Caton et al., 2007), GM-CSF receptor-deficient *Csf2a*$^{-/-}$ mice (Robb et al., 1995), *Flt3*$^{-/-}$ mice (Mackarehtschian et al., 1995), TNF$\alpha^{-/-}$ mice (B6.129S-Tnf^{tm1Gkl}/J) (Pasparakis et al., 1996), and OT II TCR transgenic mice harboring OVA-specific CD4$^+$ T cells (Barnden et al., 1998); all mice were backcrossed against a C57BL/6 background. Mixed [DTR > WT] BM chimeras were generated as reported (Varol et al., 2007). After BM transfer, the recipients were allowed to rest for 8 weeks before use. All mice were maintained under specific pathogen-free conditions and handled according to protocols approved by the Weizmann Institute Animal Care Committee as per international guidelines.

Isolation of MDPs, Pre-cDCs, and BM Monocytes

BM cells were harvested from the femora and tibiae of *Cx$_3$cr1*$^{gfp/+}$ CD45.1, CD45.1 C57BL/6 WT mice or CD11c-cre/Rosa26-tdRFP mice and enriched for mononuclear cells on a Ficoll density gradient. The cells were then immunostained with anti-CD117-PE, anti-CD11b-PerCP, and anti-Gr1 (Ly6C/G)-APC, fluorochrome-conjugated antibodies. MDPs were identified as CX$_3$CR1/GFP$^+$ CD117$^+$ cells negative for CD11b and Ly6C. Cells were purified by high-speed sorting with a FACS Aria (Beckton-Dickinson) and injected intravenously (i.v.) into congenic CD45.2 DTx-treated [CD11c-DTR > WT] BM chimeras. Ly6C^{hi} BM monocytes were isolated by sorting of Ly6C^{hi}CD11b^{hi}cKit$^-$ CX$_3$CR1-GFP$^+$ BM cells. Ly6C^{lo} BM monocytes were defined as Ly6C^{lo}CD11b^{hi}cKit$^-$ CX$_3$CR1-GFP^{hi} BM cells. Pre-cDCs were isolated by sorting of Lin$^-$ CD11c^{hi} MHCII$^-$ CX$_3$CR1-GFP$^+$ BM cells (Lin: CD3, NK1.1, B220, CD19, and TER119).

Reconstitution of DC-Depleted Lamina Propria

For systemic DC depletion, [CD11c-DTR > WT] BM chimeras were inoculated i.p. a day before precursor engraftment and then every other day with 8 ng/gram body weight DTx (Sigma D-2918) (Varol et al., 2007; Zaft et al., 2005). Unless indicated otherwise, 0.2 ml PBS containing the purified respective cell populations were injected into the tail vein in the following amounts: 1.5 × 10^6 BM Ly6C^{hi} monocytes, 1 × 10^6 BM Ly6C^{lo} monocytes, 2 × 10^{5}MDPs, and 1 × 10^5 pre-cDCs.

GM-CSF and Flt3L Treatments

The GM-CSF and Flt3L effects were examined by subcutaneous inoculation of B16 tumor cells (7 × 10^6) that had been manipulated to overexpress GM-CSF or Flt3L (Mach et al., 2000). For testing the effects of GM-CSF and Flt3L on endogenous precursors, DTx-treated BM chimeras that were left to self-reconstitute were daily injected with the cell-culture supernatant (0.2 ml, i.p.) of B16, B16-GM-CSF, or B16-Flt3L tumor cells.

Analysis of In Vivo T Cell Priming

TCR transgenic T cells were isolated from spleens and LNs of CD45.1 OT-II mice, enriched by MACS cell sorting in accordance with the manufacturer's instructions (Miltenyi Biotec GmbH), and labeled with Carboxy Fluorescein Succinimidyl Ester (CFSE, C-1157; Invitrogen) (Jung et al., 2002). T cells (3 × 10^6/mouse) were injected into the tail veins of congenic BM chimeras (CD45.2) that had received a monocyte graft 7 days earlier. Recipient mice were challenged a day later by gavage with soluble OVA (100 mg; Sigma Aldrich).

Analysis of Recipient Mice and Flow Cytometry

Small intestinal and colonic lamina propria cells were isolated with a technique previously described (Denning et al., 2007). MLNs and Peyer's patches cells were obtained after collagenase type IV treatment (1.5 mg/ml; Sigma).

Individual villi were collected by shaving with a razor under the binocular and lamina propria cells were further isolated, as described above. Fluorochrome-labeled monoclonal antibodies (PharMingen, eBioscience, and BioLegend) were used in accordance with the manufacturer's instructions. Cells were analyzed with a FACS Calibur cytometer (Beckton-Dickinson), with CellQuest software (Beckton-Dickinson).

Induction and Analysis of Intestinal Transepithelial Dendrites

DC-depleted mice were reconstituted with WT Ly6C^{hi} monocytes for 14 days, as described. To boost transepithelial dendrite (TED) development mice were 18 hr prior to analysis treated by gavage with a TLR7 agonist (Invitrogen, C-TLRL-IMQ) (20 μg). Tissue was stained with CMTMR (CellTracker, 0.1 μM; Invitrogen) and examined for TEDs with a Zeiss confocal microscope and LSM software.

DSS-Induced Colitis Model and Murine Colonoscopy

Mice received one cycle (7 days) of dextran sulfate sodium salt (DSS) (MP Biomedicals, C-160110) treatment (1% in drinking water). To monitor colitis, we used a high-resolution murine video endoscopic system, consisting of a miniature probe (1.9 mm outer diameter), a xenon light source, a triple chip camera, and an air pump ("Coloview," Karl Storz) to achieve regulated inflation of the mouse colon. Digitally recorded video files were processed with Windows Movie Maker software (Microsoft). Endoscopic quantification of colitis was graded as described (Becker et al., 2006; Becker et al., 2005). Reconstitution kinetics in individual mice were determined by fluorescent colonoscopy performed by intrarectal insertion of a 650 μm diameter fluorescent microendoscope with the Cell-vizio system (Mauna Kea Technologies).

Histology and Immunohistochemistry

Freshly isolated terminal ileum and colon tissues were directly observed on a slide with a Zeiss Axioscope II fluorescent microscope, a confocal Zeiss microscope, or a two-photon microscope after longitudinal opening. Image acquisition was conducted with simple PCI, LSM, and Velocity software. For histology, tissues were fixed in 4% paraformaldehyde overnight at room temperature, embedded in paraffin, serially sectioned (4 μm), and stained with hematoxylin and eosin (Sigma).

Salmonella Infection and Quantitation of Bacterial Load

The isogenic *Salmonella* variant ΔTTSS-1 SB161 (Δ*invG*) was grown with low aeration for 12 hr at 37°C in LB broth (0.3 M NaCl; containing 50 μg/ml ampicillin [Sigma Aldrich]), diluted 1:20 in the same medium, grown for another 4 hr (late log phase), washed twice, and suspended in cold PBS (5×10^6 CFU/50 μl for gavage) as described (Hapfelmeier et al., 2008). DC-depleted mice were reconstituted with monocytes 7 days before gavage with 20 mg of streptomycin (Sigma Aldrich) as described (Barthel et al., 2003). DTx was given every second day during the first week. At 24 hr after streptomycin pretreatment, the mice were inoculated with 5×10^5 CFU of ΔTTSS-1 *S. typhimurium* (late log phase culture) by gavage. Fresh colon tissues were isolated 3 days after infection and homogenized with the Dispomix system (Medic Tools). Live bacterial loads of colon were determined as described previously.

Semiquantitative RT-PCR

Total RNA was extracted from murine colons with PerfectPure RNA Tissue Kit (5 PRIME). cDNA was prepared by reverse transcription of 2 μg of total RNA sample. Total RNA was reverse transcribed with a mixture of random primers and oligo-dT with a High-Capacity cDNA Reverse Transcription Kit (Applied Biosystems). cDNA was amplified by PCR with REDTaq ReadyMix (Sigma-Aldrich). The following primers were used: IL-12p40 forward, 5′-GGAGACCC TGCCCATTGAACT-3′; IL-12p40 reverse, 5′-CAACGTTGCATCCTAGGATC G-3′; HPRT1 forward, 5′-TCCAACACTTCGAGAGGTCC-3′; and HPRT1 reverse, 5′-GGGGGCTATAAGTTCTTTGC-3′. The conditions for amplification were as follows: 95°C for 2 min, 95°C for 40 s, 55°C for 40 s, 72°C for 2 min and 30 s (95°C→55°C→ 72°C: 27-33 cycles), and 72°C for 5 min.

Statistical Analysis

The results were analyzed by two-tailed unpaired Student's t test, and are expressed as means ± SEM.

SUPPLEMENTAL DATA

Supplemental Data include ten figures, one table, and two movies and can be found with this article online at http://www.cell.com/immunity/supplemental/S1074-7613(09)00362-8.

ACKNOWLEDGMENTS

We thank A. Mahler and the Jung laboratory for critical reading of the manuscript and are grateful to Y. Chermesh and O. Amram for animal husbandry. We thank Z. Eshhar and Z. Halpern for establishing the endoscopy suite, B. Reizis for sharing his CD11c-Cre mice, N. Shpigel for providing *Tnf*$^{-/-}$ mice, and M. Manz for providing *Flt3*$^{-/-}$ BM. We are grateful to V. Temper, Hadassah-Hebrew University Medical Center, for *Salmonella* typing and E. Ariel and A. Sharp for help with flow cytometry. This work was supported by the Israel Science Foundation, the MINERVA foundation, and the Fritz Thyssen Stiftung (S.J.). A.V.-E. was supported by the Association of the Swiss Friends of the Weizmann Institute. S.J. is the incumbent of the Pauline Recanati Career Development Chair.

Received: January 7, 2009
Revised: May 31, 2009
Accepted: June 22, 2009
Published online: September 3, 2009

REFERENCES

Abe, K., Nguyen, K.P., Fine, S.D., Mo, J.H., Shen, C., Shenouda, S., Corr, M., Jung, S., Lee, J., Eckmann, L., and Raz, E. (2007). Conventional dendritic cells regulate the outcome of colonic inflammation independently of T cells. Proc. Natl. Acad. Sci. USA *104*, 17022–17027.

Artis, D. (2008). Epithelial-cell recognition of commensal bacteria and maintenance of immune homeostasis in the gut. Nat. Rev. Immunol. *8*, 411–420.

Atarashi, K., Nishimura, J., Shima, T., Umesaki, Y., Yamamoto, M., Onoue, M., Yagita, H., Ishii, N., Evans, R., Honda, K., and Takeda, K. (2008). ATP drives lamina propria T(H)17 cell differentiation. Nature *455*, 808–812.

Barnden, M.J., Allison, J., Heath, W.R., and Carbone, F.R. (1998). Defective TCR expression in transgenic mice constructed using cDNA-based alpha- and beta-chain genes under the control of heterologous regulatory elements. Immunol. Cell Biol. *76*, 34–40.

Barthel, M., Hapfelmeier, S., Quintanilla-Martinez, L., Kremer, M., Rohde, M., Hogardt, M., Pfeffer, K., Russmann, H., and Hardt, W.D. (2003). Pretreatment of mice with streptomycin provides a Salmonella enterica serovar Typhimurium colitis model that allows analysis of both pathogen and host. Infect. Immun. *71*, 2839–2858.

Becker, C., Fantini, M.C., and Neurath, M.F. (2006). High resolution colonoscopy in live mice. Nat. Protoc. *1*, 2900–2904.

Becker, C., Fantini, M.C., Wirtz, S., Nikolaev, A., Kiesslich, R., Lehr, H.A., Galle, P.R., and Neurath, M.F. (2005). In vivo imaging of colitis and colon cancer development in mice using high resolution chromoendoscopy. Gut *54*, 950–954.

Becker, C., Wirtz, S., Blessing, M., Pirhonen, J., Strand, D., Bechthold, O., Frick, J., Galle, P.R., Autenrieth, I., and Neurath, M.F. (2003). Constitutive p40 promoter activation and IL-23 production in the terminal ileum mediated by dendritic cells. J. Clin. Invest. *112*, 693–706.

Berndt, B.E., Zhang, M., Chen, G.H., Huffnagle, G.B., and Kao, J.Y. (2007). The role of dendritic cells in the development of acute dextran sulfate sodium colitis. J. Immunol. *179*, 6255–6262.

Caton, M.L., Smith-Raska, M.R., and Reizis, B. (2007). Notch-RBP-J signaling controls the homeostasis of CD8- dendritic cells in the spleen. J. Exp. Med. *204*, 1653–1664.

Chieppa, M., Rescigno, M., Huang, A.Y., and Germain, R.N. (2006). Dynamic imaging of dendritic cell extension into the small bowel lumen in response to epithelial cell TLR engagement. J. Exp. Med. *203*, 2841–2852.

Coombes, J.L., and Powrie, F. (2008). Dendritic cells in intestinal immune regulation. Nat. Rev. Immunol. *8*, 435–446.

Coombes, J.L., Siddiqui, K.R., Arancibia-Carcamo, C.V., Hall, J., Sun, C.M., Belkaid, Y., and Powrie, F. (2007). A functionally specialized population of mucosal CD103+ DCs induces Foxp3+ regulatory T cells via a TGF-beta and retinoic acid-dependent mechanism. J. Exp. Med. *204*, 1757–1764.

Cooper, H.S., Murthy, S.N., Shah, R.S., and Sedergran, D.J. (1993). Clinicopathologic study of dextran sulfate sodium experimental murine colitis. Lab. Invest. *69*, 238–249.

Daro, E., Pulendran, B., Brasel, K., Teepe, M., Pettit, D., Lynch, D.H., Vremec, D., Robb, L., Shortman, K., McKenna, H.J., et al. (2000). Polyethylene glycol-modified GM-CSF expands CD11b(high)CD11c(high) but notCD11b(low)CD11c(high) murine dendritic cells in vivo: A comparative analysis with Flt3 ligand. J. Immunol. *165*, 49–58.

Denning, T.L., Wang, Y.C., Patel, S.R., Williams, I.R., and Pulendran, B. (2007). Lamina propria macrophages and dendritic cells differentially induce regulatory and interleukin 17-producing T cell responses. Nat. Immunol. *8*, 1086–1094.

Fogg, D.K., Sibon, C., Miled, C., Jung, S., Aucouturier, P., Littman, D.R., Cumano, A., and Geissmann, F. (2006). A clonogenic bone marrow progenitor specific for macrophages and dendritic cells. Science *311*, 83–87.

Garrett, W.S., Lord, G.M., Punit, S., Lugo-Villarino, G., Mazmanian, S.K., Ito, S., Glickman, J.N., and Glimcher, L.H. (2007). Communicable ulcerative colitis induced by T-bet deficiency in the innate immune system. Cell *131*, 33–45.

Geissmann, F., Jung, S., and Littman, D.R. (2003). Blood monocytes consist of two principal subsets with distinct migratory properties. Immunity *19*, 71–82.

Hapfelmeier, S., Muller, A.J., Stecher, B., Kaiser, P., Barthel, M., Endt, K., Eberhard, M., Robbiani, R., Jacobi, C.A., Heikenwalder, M., et al. (2008). Microbe sampling by mucosal dendritic cells is a discrete, MyD88-independent step in DeltainvG S. Typhimurium colitis. J. Exp. Med. *205*, 437–450.

Hieronymus, T., Gust, T.C., Kirsch, R.D., Jorgas, T., Blendinger, G., Goncharenko, M., Supplitt, K., Rose-John, S., Muller, A.M., and Zenke, M. (2005). Progressive and controlled development of mouse dendritic cells from Flt3+CD11b+ progenitors in vitro. J. Immunol. *174*, 2552–2562.

Iijima, N., Linehan, M.M., Saeland, S., and Iwasaki, A. (2007). Vaginal epithelial dendritic cells renew from bone marrow precursors. Proc. Natl. Acad. Sci. USA *104*, 19061–19066.

Iwasaki, A. (2007). Mucosal dendritic cells. Annu. Rev. Immunol. *25*, 381–418.

Jaensson, E., Uronen-Hansson, H., Pabst, O., Eksteen, B., Tian, J., Coombes, J.L., Berg, P.L., Davidsson, T., Powrie, F., Johansson-Lindbom, B., and Agace, W.W. (2008). Small intestinal CD103+ dendritic cells display unique functional properties that are conserved between mice and humans. J. Exp. Med. *205*, 2139–2149.

Jakubzick, C., Tacke, F., Ginhoux, F., Wagers, A.J., van Rooijen, N., Mack, M., Merad, M., and Randolph, G.J. (2008). Blood monocyte subsets differentially give rise to CD103+ and CD103- pulmonary dendritic cell populations. J. Immunol. *180*, 3019–3027.

Jang, M.H., Sougawa, N., Tanaka, T., Hirata, T., Hiroi, T., Tohya, K., Guo, Z., Umemoto, E., Ebisuno, Y., Yang, B.G., et al. (2006). CCR7 is critically important for migration of dendritic cells in intestinal lamina propria to mesenteric lymph nodes. J. Immunol. *176*, 803–810.

Jung, S., Aliberti, J., Graemmel, P., Sunshine, M.J., Kreutzberg, G.W., Sher, A., and Littman, D.R. (2000). Analysis of fractalkine receptor CX(3)CR1 function by targeted deletion and green fluorescent protein reporter gene insertion. Mol. Cell. Biol. *20*, 4106–4114.

Jung, S., Unutmaz, D., Wong, P., Sano, G., De los Santos, K., Sparwasser, T., Wu, S., Vuthoori, S., Ko, K., Zavala, F., et al. (2002). In vivo depletion of CD11c(+) dendritic cells abrogates priming of CD8(+) T cells by exogenous cell-associated antigens. Immunity *17*, 211–220.

Karsunky, H., Merad, M., Cozzio, A., Weissman, I.L., and Manz, M.G. (2003). Flt3 ligand regulates dendritic cell development from Flt3+ lymphoid and myeloid-committed progenitors to Flt3+ dendritic cells in vivo. J. Exp. Med. *198*, 305–313.

Landsman, L., Varol, C., and Jung, S. (2007). Distinct differentiation potential of blood monocyte subsets in the lung. J. Immunol. *178*, 2000–2007.

Liu, K., Victora, G.D., Schwickert, T.A., Guermonprez, P., Meredith, M.M., Yao, K., Chu, F.F., Randolph, G.J., Rudensky, A.Y., and Nussenzweig, M. (2009). In vivo analysis of dendritic cell development and homeostasis. Science *324*, 392–397.

Liu, K., Waskow, C., Liu, X., Yao, K., Hoh, J., and Nussenzweig, M. (2007). Origin of dendritic cells in peripheral lymphoid organs of mice. Nat. Immunol. *8*, 578–583.

Luche, H., Weber, O., Nageswara Rao, T., Blum, C., and Fehling, H.J. (2007). Faithful activation of an extra-bright red fluorescent protein in "knock-in" Cre-reporter mice ideally suited for lineage tracing studies. Eur. J. Immunol. *37*, 43–53.

Mach, N., Gillessen, S., Wilson, S.B., Sheehan, C., Mihm, M., and Dranoff, G. (2000). Differences in dendritic cells stimulated in vivo by tumors engineered to secrete granulocyte-macrophage colony-stimulating factor or Flt3-ligand. Cancer Res. *60*, 3239–3246.

Mackarehtschian, K., Hardin, J.D., Moore, K.A., Boast, S., Goff, S.P., and Lemischka, I.R. (1995). Targeted disruption of the flk2/flt3 gene leads to deficiencies in primitive hematopoietic progenitors. Immunity *3*, 147–161.

Miller, G., Pillarisetty, V.G., Shah, A.B., Lahrs, S., and DeMatteo, R.P. (2003). Murine Flt3 ligand expands distinct dendritic cells with both tolerogenic and immunogenic properties. J. Immunol. *170*, 3554–3564.

Miller, G., Pillarisetty, V.G., Shah, A.B., Lahrs, S., Xing, Z., and DeMatteo, R.P. (2002). Endogenous granulocyte-macrophage colony-stimulating factor overexpression in vivo results in the long-term recruitment of a distinct dendritic cell population with enhanced immunostimulatory function. J. Immunol. *169*, 2875–2885.

Naik, S.H., Metcalf, D., van Nieuwenhuijze, A., Wicks, I., Wu, L., O'Keeffe, M., and Shortman, K. (2006). Intrasplenic steady-state dendritic cell precursors that are distinct from monocytes. Nat. Immunol. *7*, 663–671.

Niess, J.H., Brand, S., Gu, X., Landsman, L., Jung, S., McCormick, B.A., Vyas, J.M., Boes, M., Ploegh, H.L., Fox, J.G., et al. (2005). CX3CR1-mediated dendritic cell access to the intestinal lumen and bacterial clearance. Science *307*, 254–258.

Okayasu, I., Hatakeyama, S., Yamada, M., Ohkusa, T., Inagaki, Y., and Nakaya, R. (1990). A novel method in the induction of reliable experimental acute and chronic ulcerative colitis in mice. Gastroenterology *98*, 694–702.

Onai, N., Obata-Onai, A., Schmid, M.A., Ohteki, T., Jarrossay, D., and Manz, M.G. (2007). Identification of clonogenic common Flt3+M-CSFR+ plasmacytoid and conventional dendritic cell progenitors in mouse bone marrow. Nat. Immunol. *8*, 1207–1216.

Pasparakis, M., Alexopoulou, L., Episkopou, V., and Kollias, G. (1996). Immune and inflammatory responses in TNF alpha-deficient mice: A critical requirement for TNF alpha in the formation of primary B cell follicles, follicular dendritic cell networks and germinal centers, and in the maturation of the humoral immune response. J. Exp. Med. *184*, 1397–1411.

Rescigno, M., Urbano, M., Valzasina, B., Francolini, M., Rotta, G., Bonasio, R., Granucci, F., Kraehenbuhl, J.P., and Ricciardi-Castagnoli, P. (2001). Dendritic cells express tight junction proteins and penetrate gut epithelial monolayers to sample bacteria. Nat. Immunol. *2*, 361–367.

Robb, L., Drinkwater, C.C., Metcalf, D., Li, R., Kontgen, F., Nicola, N.A., and Begley, C.G. (1995). Hematopoietic and lung abnormalities in mice with a null mutation of the common beta subunit of the receptors for granulocyte-macrophage colony-stimulating factor and interleukins 3 and 5. Proc. Natl. Acad. Sci. USA *92*, 9565–9569.

Sun, C.M., Hall, J.A., Blank, R.B., Bouladoux, N., Oukka, M., Mora, J.R., and Belkaid, Y. (2007). Small intestine lamina propria dendritic cells promote de novo generation of Foxp3 T reg cells via retinoic acid. J. Exp. Med. *204*, 1775–1785.

Uematsu, S., Fujimoto, K., Jang, M.H., Yang, B.G., Jung, Y.J., Nishiyama, M., Sato, S., Tsujimura, T., Yamamoto, M., Yokota, Y., et al. (2008). Regulation of humoral and cellular gut immunity by lamina propria dendritic cells expressing Toll-like receptor 5. Nat. Immunol. *9*, 769–776.

Vallon-Eberhard, A., Landsman, L., Yogev, N., Verrier, B., and Jung, S. (2006). Transepithelial pathogen uptake into the small intestinal lamina propria. J. Immunol. *176*, 2465–2469.

Varol, C., Landsman, L., Fogg, D.K., Greenshtein, L., Gildor, B., Margalit, R., Kalchenko, V., Geissmann, F., and Jung, S. (2007). Monocytes give rise to mucosal, but not splenic, conventional dendritic cells. J. Exp. Med. *204*, 171–180.

Vasquez, N., Mangin, I., Lepage, P., Seksik, P., Duong, J.P., Blum, S., Schiffrin, E., Suau, A., Allez, M., Vernier, G., et al. (2007). Patchy distribution of mucosal lesions in ileal Crohn's disease is not linked to differences in the dominant mucosa-associated bacteria: A study using fluorescence in situ hybridization and temporal temperature gradient gel electrophoresis. Inflamm. Bowel Dis. *13*, 684–692.

Waskow, C., Liu, K., Darrasse-Jeze, G., Guermonprez, P., Ginhoux, F., Merad, M., Shengelia, T., Yao, K., and Nussenzweig, M. (2008). The receptor tyrosine kinase Flt3 is required for dendritic cell development in peripheral lymphoid tissues. Nat. Immunol. *9*, 676–683.

Worbs, T., Bode, U., Yan, S., Hoffmann, M.W., Hintzen, G., Bernhardt, G., Forster, R., and Pabst, O. (2006). Oral tolerance originates in the intestinal immune system and relies on antigen carriage by dendritic cells. J. Exp. Med. *203*, 519–527.

Xavier, R.J., and Podolsky, D.K. (2007). Unravelling the pathogenesis of inflammatory bowel disease. Nature *448*, 427–434.

Zaft, T., Sapoznikov, A., Krauthgamer, R., Littman, D.R., and Jung, S. (2005). CD11chigh dendritic cell ablation impairs lymphopenia-driven proliferation of naive and memory CD8+ T cells. J. Immunol. *175*, 6428–6435.